Self-Curing Decoupling Technique for MIMO Antenna Arrays in Mobile Terminals

Jiangwei Sui, Yuhang Dou, *Student Member, IEEE*, Xide Mei, and Ke-Li Wu, *Fellow, IEEE*

***Abstract*— The self-curing decoupling technique is substantially extended to apply to multi-input multi-output (MIMO) antenna arrays in mobile terminals. Using this proposed technique, the mutual coupling between antennas can be reduced by inlaying lumped element capacitors on the ground plane. The decoupling method does not require any physical connection or obstruction between coupled antennas. The significance of the proposed decoupling technique is fourfold: 1) it works for inverted-F antennas (IFAs), monopole antennas, and loop antennas, the most three commonly used antenna forms for mobile terminals; 2) the inherent improvement on matching conditions after decoupling; 3) the flexibility in implementation owing to its detachment from the antenna body; and 4) the applicability to an array with more than two elements. Four demonstrating examples, including two IFAs, two monopole antennas, two loop antennas, and a MIMO array with four elements of different antenna types are studied by EM modeling, passive tests, and MIMO over-the-air (OTA) measurements. The experimental results show that significant improvements in port isolation (from 9 to 30 dB), total efficiency (from 53% to 69%), and above all, the system data throughput can be achieved. The working mechanism of the method is revealed and justified through the partial element equivalent circuit (PEEC) model in the fifth example.**

***Index Terms*— Antenna array, data throughput, decoupling technique, long-term evolution (LTE), multi-input multi-output (MIMO), mutual coupling, over-the-air (OTA) test, terminal antennas.**

I. Introduction

MULTI-INPUT multi-output (MIMO) technology has been widely used in today's wireless communication systems, from base stations to Wi-Fi modules and various mobile terminals such as smartphones and tablets. It has become an essential component of the industry standards, not only in IEEE 802.11n and long-term evolution (LTE) 4G but also in 5G wireless systems. By using multiple antennas, a MIMO system sends and receives more than one data signal streams simultaneously over the same radio channel by utilizing uncorrelated channel paths in a multipath environment. To accommodate the high demands of a high number of antennas on a smartphone, new design challenges must be confronted. One of the thorny issues is how to reduce the mutual coupling among tightly packed antennas that are attached to a compact circuit board, which is full of densely populated surface mounted electronic components.

There are mainly three basic commonly seen antenna forms on a wireless terminal: inverted-F antennas (IFAs), monopole antennas, and loop antennas [1]. A common design scenario is that due to the compact space in a terminal, severe mutual couplings are inevitable among antennas. It has been well understood that mutual coupling will significantly degrade the data throughput in a MIMO system [2] in addition to the decisive influence of spatial correlation. The impact of mutual coupling can be attributed by three factors: 1) it lowers the total efficiency of the antenna array as the coupled antenna dissipates the coupled energy; 2) it increases the correlation of different channels and deteriorates the MIMO performance; and 3) it decreases the signal-to-noise (S/N) ratio of each communication channel [3]. Recent research reveals that a coupled signal also degrades the linearity of the power amplifier in the victim receiver [4].

Tremendous research efforts have been devoted to mitigating mutual coupling between antennas in a mobile terminal. In [5], several multiple-IFA configurations for mobile handsets are investigated to show that the relative position of the antennas may be optimized to obtain low mutual coupling. The polarization diversity between antennas can also be utilized to improve antenna isolation [6]. A neutralization line that connects two coupled IFAs [7] or monopole antennas [8] can be introduced to neutralize the mutual admittance. Inserting a parasitic element [9]–[11] or decoupling element [12] between antennas is also an effective approach to achieve good isolation if space permits. Besides, destructed ground plane structures [13], [14] or electromagnetic band-gap structures [15], [16] can be introduced between coupled antennas to reduce the mutual coupling by manipulating the surface wave or the current flowing on the ground plane.

Another category of decoupling techniques shunt connects the coupled antennas with a decoupling circuit, which can be a transmission line circuit [17], [18], an *LC* circuit [19], [20], a coupler [21]–[23], or a coupled resonator circuit [24]–[26]. Two major challenges are faced by these techniques for mobile terminal applications. First, the circuits need to be physically connected to the antennas with appropriate phase control, which is not convenient in a practical mobile phone. Second, the footprints of these circuits, including the connecting

Manuscript received December 31, 2018; revised June 23, 2019; accepted September 14, 2019. Date of publication September 30, 2019; date of current version February 3, 2020. This work was supported in part by the Research Grants Council of the Hong Kong Special Administrative Region, China, under Grant 14205217. *(Corresponding author: Ke-Li Wu.)*

J. Sui was with the Department of Electronic Engineering, The Chinese University of Hong Kong, Hong Kong. He is now with Vivo Communication Technology Co., Ltd. (e-mail: jwsui@ee.cuhk.edu.hk).

Y. Dou, X. Mei, and K.-L. Wu are with the Department of Electronic Engineering, The Chinese University of Hong Kong, Hong Kong (e-mail: yhdou@ee.cuhk.edu.hk; xdmei@ee.cuhk.edu.hk; klwu@cuhk.edu.hk).

Color versions of one or more of the figures in this article are available online at http://ieeexplore.ieee.org.

Digital Object Identifier 10.1109/TAP.2019.2943410

TABLE I
COMPARISON OF THE PROPOSED TECHNIQUE WITH PRIOR WORKS

	Decoupling Method	Applicable Antenna Types	Obstruction or Connection between Antennas	Matching Condition	Size of Decoupling Structure (λ)	No. of Antennas
[11][2014] [12][2017]	Parasitic Element	Monopole, Loop, IFA	Yes	Deteriorated	0.21	2 or more
[13][2007]	Defected Ground Structure	PIFA, Monopole	Yes	Deteriorated	0.32	2
[24][2014]	Decoupling Circuit	IFA, Monopole	Yes	Deteriorated	0.13	2
[27][2018]	Self-Curing for IFAs	Only IFA	No	Deteriorated	0.04	2
This Work	This New Self-Curing	Monopole, Loop, IFA	No	Improved or Maintained	0.036	2 or more

transmission lines, are usually in the order of half a wavelength, which is too extravagant in terms of electrical dimensions to be adopted in mobile terminal applications.

Recently, a self-curing decoupling technique is proposed by Sui and Wu [27] to decouple two IFAs in a mobile terminal, by which mutual coupling can be significantly cancelled out by adding a capacitor between the ground and a short stub extruded from the shorting arm of an IFA. However, the previous technique fails on monopole and loop antennas. The main reason is that the capacitor has to be attached to the antenna body and severely changes the current distribution on the monopole and loop antennas. Another unpleasant drawback of the previous technique is that the matching condition of the decoupled IFAs will be substantially deteriorated, which will increase the design complexity of a MIMO antenna array. What is more, the mathematical model presented in [27] only applies to two IFAs, which is far from sufficient for a general MIMO antenna array case with more antenna elements and different antenna types.

In this article, the self-curing decoupling technique is substantially extended to MIMO antenna arrays in a mobile terminal. The proposed technique works equally well for IFA, monopole antenna, and loop antenna. Unlike the previously presented technique in [27], in which a short stub connecting a grounded capacitor needs to be tapped to the shorting arm of an IFA, one or more decoupling capacitors in this proposed self-curing decoupling technique are inlaid on the ground plane at "acupoints" without physical attachment to the antennas. With little perturbation on the current distribution of the antennas, the proposed self-curing decoupling method attributes the following attractive and unique features: 1) it is versatile for all the commonly used antennas on wireless terminals: i.e., IFA, monopole antenna, and loop antenna; 2) it improves the matching conditions of the decoupled antennas without needing any extra impedance matching circuit; 3) it is highly flexible in implementation as the decoupling capacitors occupy nearly no real estate and are not connected to the antennas; and 4) it can be easily applied to MIMO antenna arrays with more than two antenna elements. The main features of the proposed self-curing decoupling technique and the major prior art are compared in Table I. It can be seen that the self-curing technique is far superior to the existing techniques, including the self-curing decoupling technique that is dedicated for IFAs.

What is more, the physical mechanism of the proposed technique is revealed using the partial element equivalent circuit (PEEC) model. PEEC is a rigorous EM model in the circuit domain. It is an effective tool to interpret an EM problem from a circuit point of view. It is shown that the inlaid capacitor at an "acupoint" on the ground plane naturally creates an equivalent coherent current source. The current source generates the interference signal that is of the same magnitude but opposite phase as those of the coupled signal at the coupled antenna port, resulting in mutual coupling cancelation.

This article is organized as follows. Section II introduces the decoupling scheme of the proposed technique. Four proof-of-concept examples are given in Section III. The significance of the decoupling technique is demonstrated through not only passive antenna measurements but also active MIMO over-the-air (OTA) throughput measurements in a multi-path channel anechoic chamber. The physical mechanism of the decoupling method is numerically justified by PEEC modeling in Section IV. Finally, the conclusion is given in Section V.

II. DECOUPLING SCHEME

As shown in Fig. 1(a), N antennas are co-located above the same ground plane with inevitable mutual couplings. Fig. 1(b) shows the schematic of the proposed technique, in which M decoupling capacitors are inlaid at the "acupoints" on the ground plane. Generally, M is less than or equal to N. The antennas can be IFAs, monopole antennas, or loop antennas, or any combination of them. Different from the previous method [27], in which the decoupling capacitor is attached to the shorting arm of an IFA, the decoupling capacitors in this technique are inlaid on the ground plane near the edge. The shallow cuts for inlaying decoupling capacitors are on the edge of the ground plane, and their size is typically as small as 2–4 mm^2.

To find the optimal positions and the values for the M decoupling capacitors, M auxiliary ports are defined, as shown in Fig. 1(c). Fig. 2 shows the network description of the proposed decoupling scheme. Unlike the simple network description used in [27], in which two identical capacitive loads

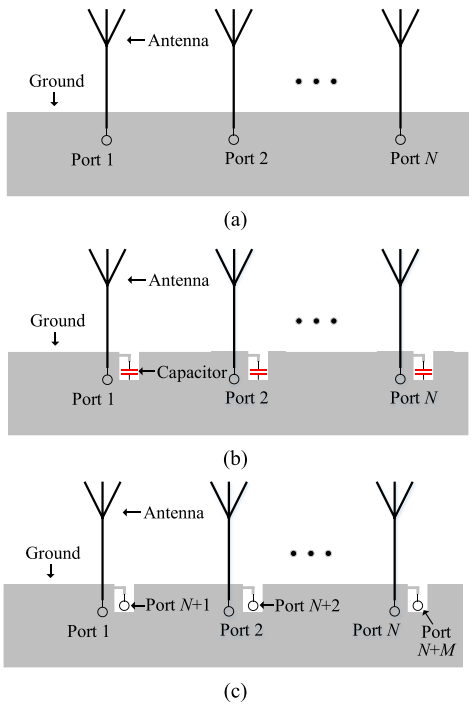

Fig. 1. Scheme of the proposed decoupling technique. (a) Coupled antennas. (b) Decoupled antennas. (c) Auxiliary ports for designing decoupling capacitors.

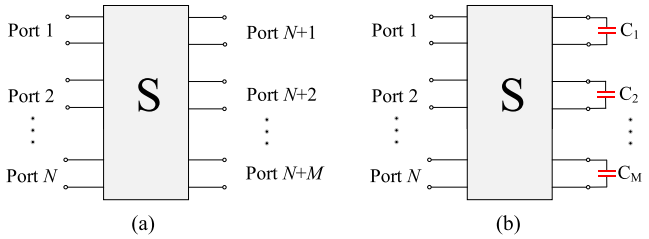

Fig. 2. Network description of the decoupling method. (a) (N + M) port network. (b) N-port network with M ports terminated by capacitors.

are assumed for two antennas, the N antennas in a general decoupling problem are described by the following N × N S-parameter matrix with M ports terminated by capacitors, as shown in Fig. 2(b):

$$S = \begin{pmatrix} S_{11} & \cdots & S_{1N} \\ \vdots & \ddots & \vdots \\ S_{N1} & \cdots & S_{NN} \end{pmatrix}. \quad (1)$$

The decoupling problem becomes a matrix diagonalization problem for the matrix S. There are various ways to diagonalize a matrix. In this work, the nonlinear least square scheme is adopted with the following cost function $F(\boldsymbol{C})$, where variable vector $\boldsymbol{C}$ is composed of the M decoupling capacitors or $\boldsymbol{C} = [C_1, C_2, \ldots, C_M]$:

$$\min_{\boldsymbol{C}} ||F(\boldsymbol{C})||_2^2 = \min_{\boldsymbol{C}} (|S_{12}(\boldsymbol{C})|^2 + \cdots + |S_{1N}(\boldsymbol{C})|^2 + |S_{23}(\boldsymbol{C})|^2 + \cdots + |S_{N-1,N}(\boldsymbol{C})|^2). \quad (2)$$

The goal of this optimization is to find a set of capacitors that minimize all the mutual couplings.

In addition to the nonlinear least square optimization scheme, the graphical solution for the case of N = M = 2 is also very effective. It will be demonstrated in the design examples that the values for the capacitors are not necessarily the same. Such a general solution cannot be obtained using the simple network model presented in [27].

III. Demonstration Examples

In this section, the first three examples are used to study the generality of the proposed method to the three common antenna types in a mobile terminal: IFA, monopole antenna, and loop antenna. The graphical contour plot method is adopted to find the optimal capacitors. The contour plot reflects the relation of the mutual coupling and two decoupling capacitors provided that the matching condition of the two antennas is not deteriorated. In the fourth example, a four-antenna array of different antenna types is studied to demonstrate the applicability of the proposed method for an array with a high number of elements. The nonlinear least square scheme is applied to the last example to find the four optimal capacitors.

A. OTA Experimental Setup

All the demonstration cases are EM designed using HFSS and fabricated using the FR4 PCB boards. In EM simulation, the relative permittivity and the loss tangent of the FR4 substrate are set to 4.3 and 0.02, respectively. The thickness and conductivity of the copper sheet are set to 35 um and 3.4×10^7 S/m, respectively.

To study the impact of decoupling on data throughput of a two-antenna MIMO system, each pair of prototyped MIMO antennas is integrated with a commercially available two-port LTE module to constitute a complete MIMO device, which can communicate with the base station. The OTA performance of this MIMO device is measured in a MIMO OTA laboratory, which is equipped with two Anite FS8 eight-channel emulators and supports the desired spatial channel model extended (SCME) channel models, including urban microcell (UMi) and urban macrocell (UMa) channel models [28]. The detailed description of the OTA laboratory is given in [27]. To compare the OTA performance of the MIMO device with the coupled and decoupled antennas, the MIMO average-radiated SIR sensitivity (MARSS) is adopted as a figure of merit. The sensitivity is defined as the signal-to-noise ratio (SNR) value required to reach 90% of the theoretical maximum throughput of the test case [29].

In the OTA tests, the channel bandwidth is set to 10 MHz (2135–2145 MHz), and the modulation is chosen to be 64 and 16 QAM, which are with the maximum throughput of 33.356 and 14.386 Mb/s, for the tests under UMi and UMa channel models, respectively. Each throughput data is the average value repeatedly measured with the MIMO device rotated every 45° in the horizontal plane.

B. Two Inverted-F Antennas

As shown in Fig. 3(a), two IFAs are printed on the two opposite short edges of a phone-size PCB board. To decouple

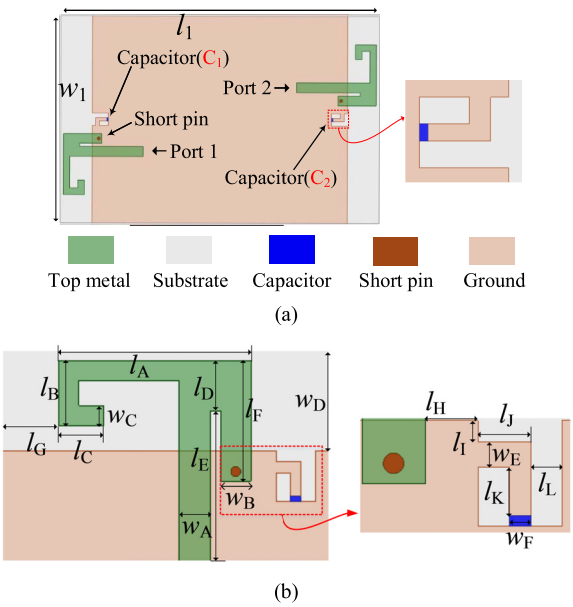

Fig. 3. Configuration of two IFAs. (a) Top view. (b) Dimensions.

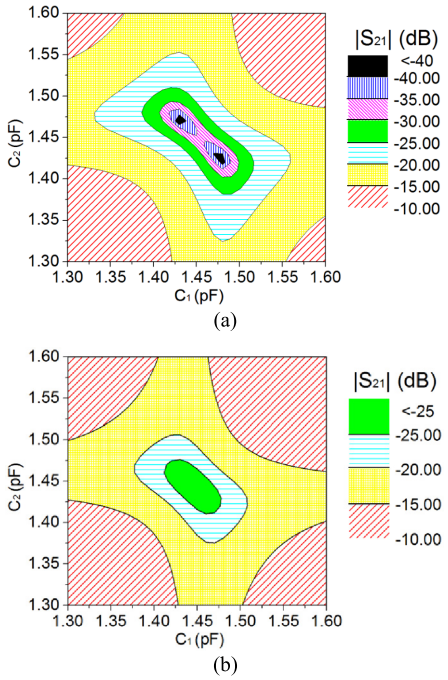

Fig. 4. Contour plot of mutual coupling S_{21} of the two IFAs with respect to C_1 and C_2 with different distances. (a) $l_H = 2.5$ mm. (b) $l_H = 6$ mm.

the two IFAs, a capacitor is inlaid in a reentrant opening on the ground plane near but not connected to the shorting arm of each IFA. The electrically shallow opening is cut from the edge of the ground plane, and a short stub is stretched from a fringe of the opening. A lumped element capacitor is soldered between the other end of the stub and the ground. The dimension of the opening should be electrically small to ensure the influence of the opening on the original attributes of antennas is negligible.

The two IFAs are designed in LTE band 1 (2.11–2.17 GHz), which the LTE module supports. The detailed dimensions are marked in Fig. 3(b) and their values are given in Table II. For the distance of $l_H = 2.5$ mm, the 2-D contour plot of the mutual coupling, at 2.14 GHz with respect to capacitances, C_1 and C_2, is presented in Fig. 4(a). It can be found that for an allowable mutual coupling, say -35 dB, there are two possible solution ranges, for C_1 and C_2: (C_1 around 1.43 pF and C_2 around 1.47 pF or C_1 around 1.47 pF and C_2 around 1.43 pF), which cannot be obtained by the method described in [27]. This example demonstrates that the graphic solution can easily provide global optimal solutions when the number of design variables is not high.

To illustrate the sensitivity of the position of the reentrant opening from its associated IFA, the contour of S_{21} at 2.14 GHz with respect to the two capacitors with distance $l_H = 6$ mm is plotted in Fig. 4(b). Although the achievable mutual coupling is worse than that of $l_H = 2.5$ mm shown in Fig. 4(a), significant mutual coupling reduction can still be seen, showing that the position of the opening is insensitive.

Fig. 5 shows a photograph of the pair of decoupled IFAs using the proposed decoupling method. The capacitors used in this article are of Murata GJM high-Q value series. Two capacitors are shunt soldered to reduce the unwanted loss. The simulated and measured S-parameters of the coupled and the decoupled IFAs are compared in Fig. 6, showing

TABLE II

PARAMETER VALUES FOR DIFFERENT ANTENNA CASES (UNIT: mm)

Inverted-F Antennas	l_1	l_A	l_B	l_C	l_D	l_E	l_F	l_G	l_H	l_I	l_J	l_K
	100	19	6.5	4.5	5	20	12	9	2.5	1	2.5	2.3
	l_L	w_1	w_A	w_B	w_C	w_D	w_E	w_F				
	1.5	65	3.1	3	2	10	1.2	1				
Monopole Antennas	l_2	l_M	l_N	l_O	l_P	l_Q	l_R	l_S	w_2	w_G	w_H	w_I
	120	19	6	28	11	1.8	1	3	70	3.1	2	10
	w_J	w_K										
	1.2	1.7										
Loop Antennas	l_3	l_T	l_U	l_V	l_W	l_X	l_Y	l_Z	w_3	w_L	w_M	w_N
	120	51.7	7.2	23	2.5	1	3.7	2.1	75	3.1	2	7
	w_O	w_P										
	1.7	1										

that the measured isolation at the center frequency 2.14 GHz is enhanced from about 12 to 29 dB, while the matching bandwidth is becoming much wider after decoupling without any extra matching circuit. The measured results are in good correlation with the EM simulated.

The radiation characteristics of the two pairs of IFAs are also experimentally investigated. The simulated and measured total efficiencies of the coupled and decoupled IFAs are presented in Fig. 7. The total efficiency for the ith antenna is defined by [30], [31]

$$\eta_{Total,i} = \left(1 - |S_{ii}|^2 - \sum_{j \neq i} |S_{ij}|^2\right) \times \eta_{Radiation,i}. \quad (3)$$

Here, $\eta_{Radiation}$ denotes the radiation efficiency of the ith antenna with other antennas terminated by matched loads.

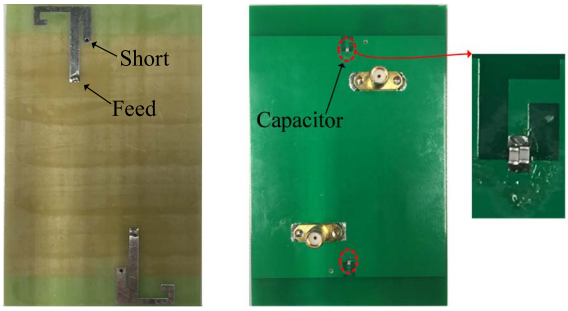

Fig. 5. Prototype of the decoupled IFAs. (a) Top view. (b) Bottom view (note that two shunt-connected surface mounted device (SMD) capacitors are used to realize one capacitor).

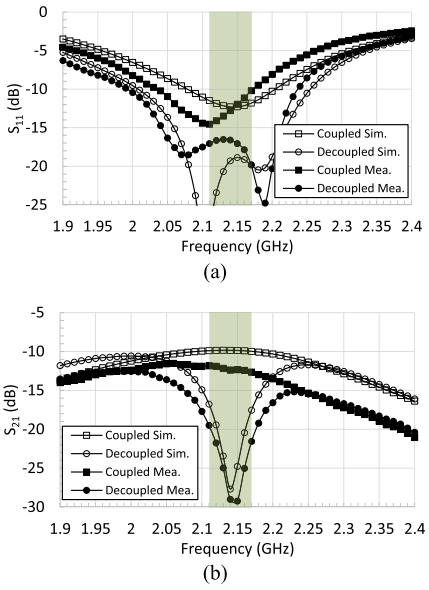

Fig. 6. Simulated and measured S-parameters of the coupled pair and decoupled pair of IFAs. (a) $|S_{11}|$. (b) $|S_{21}|$.

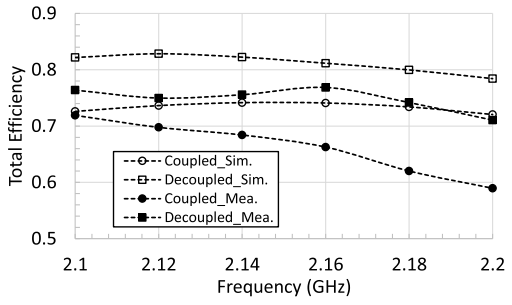

Fig. 7. Simulated and measured total efficiencies of the coupled pair and decoupled pair of IFAs.

It can be found that the total efficiency at 2.14 GHz is improved from 68% to 75% after decoupling. It is interesting to observe from Fig. 8 that the radiation patterns do not change too much after decoupling, meaning that the decoupling does not significantly change the current distribution of the original coupled antennas. The envelope correlation coefficient (ECC) and multiplexing efficiency [27] are presented in Table III. It is seen that the multiplexing efficiencies of two IFAs that take into consideration both ECC and total efficiency are improved after decoupling.

The OTA tests for the LTE module with the coupled and decoupled MIMO antennas are conducted. The average

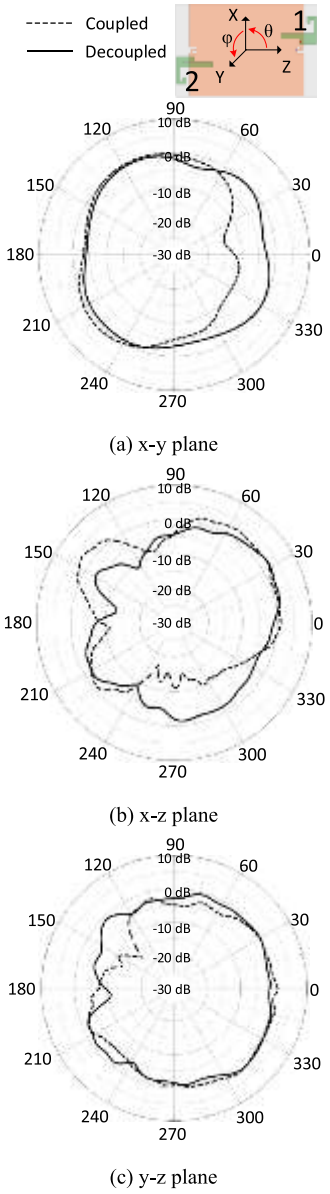

Fig. 8. Measured radiation patterns of antenna 1 in coupled and decoupled pairs of IFAs when antenna 2 is terminated with a matched load. (a) *xy* plane. (b) *xz* plane. (c) *yz* plane.

TABLE III
ECC/MULTIPLEXING EFFICIENCY OF THE THREE ANTENNA TYPES

	ECC		Multiplexing Efficiency (%)	
	Coupled	Decoupled	Coupled	Decoupled
IFA	0.036	0.0005	66.76	74.98
Monopole	0.284	0.038	44.8	67.6
Loop	0.169	0.173	45.6	49.1

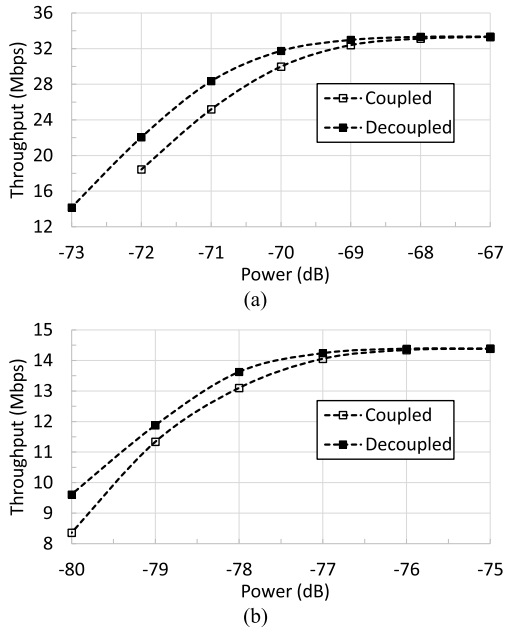

Fig. 9. Measured average throughput of the LTE module with the coupled and decoupled IFAs versus power. (a) In UMi channel environment using 64 QAM modulation. (b) In UMa channel environment using 16 QAM modulation.

throughputs for the coupled and decoupled cases under UMi and UMa environments are compared in Fig. 9(a) and (b). In the UMi channel environment, when throughput drops 10% from the maximum value to 30 Mb/s, the required power for the MIMO module with the decoupled antennas is −70.5 dBm, whereas that for the coupled antennas is −70 dBm. The 0.5 dB power reduction in MARSS means that 11% of power saving for the same MIMO performance can be achieved by employing the decoupling method. Similarly, about 0.3 dB power saving is achieved under the UMa channel environment when throughput drops from the maximum value 14.386–13 Mb/s (about 90% of the maximum value).

C. Two Monopole Antennas

Apart from IFA, a monopole antenna is also widely used in mobile terminals due to its low profile, compact size, and convenience of the layout. The proposed decoupling method is also applicable to two coupled monopole antennas. Without loss of generality, two identical monopole antennas working in LTE band 1 (2.11–2.17 GHz) are considered as a showcase. Fig. 10(a) shows the layout of two monopole antennas with two decoupling capacitors inlaid on the ground. The two monopole antennas are placed along the top edge of the PCB board symmetrically. The dimensions of the monopole antennas, as well as a reentrant opening for inlaying the decoupling capacitor, are marked in Fig. 10(b) with specific values listed in Table II. In this showcase, the electrically small reentrant opening on the ground plane is cut near the feeding line of each monopole antenna. Again, a short stub is stretched from a fringe of the opening and is terminated by a grounded lumped element capacitor.

Having picked locations for the openings along the edge of the ground plane and chosen the sizes of the opening

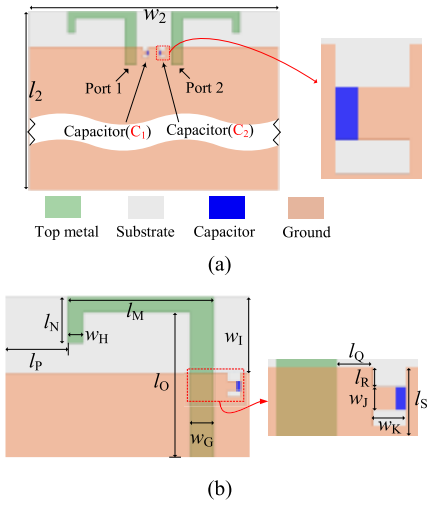

Fig. 10. Configuration of two monopole antennas. (a) Top view. (b) Dimensions.

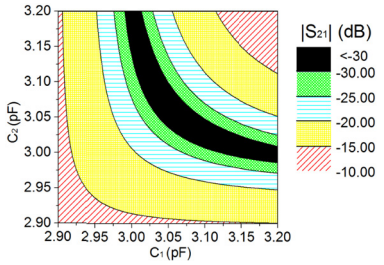

Fig. 11. Contour plot of mutual coupling S_{21} and two capacitors C_1 and C_2 for the monopole antenna case.

and the stub, a contour plot of mutual coupling at the center frequency with respect to C_1 and C_2 can be easily obtained. As shown in Fig. 11, for a given mutual coupling level, there is a solution range for the two capacitors. Obviously, the solution is not unique. Note that the contour plot is obtained based on network parameter transformation in circuit level and there is a certain slight difference with EM simulation because the effect of the capacitor size will also be considered in EM simulation so that a fine-tuning of the capacitor value is required in EM simulation. Two capacitors of 3 pF are adopted in this design after fine-tuning. The simulated and measured S-parameters are compared in Fig. 12. It can be seen that the isolation between the two monopole antennas is improved from about 9 to 30 dB at 2.14 GHz and, interestingly, the matching condition is also significantly improved. Fig. 13 shows the fabricated prototype of the pair of decoupled monopole antennas.

As listed in Table III, the multiplexing efficiency at 2.14 GHz is improved from 44.8% to 67.6% after decoupling. The average throughputs for the LTE module with the coupled and decoupled monopole antennas are measured under UMi and UMa environments, and the results are presented in Table IV. In the UMi channel environment, to achieve the same 90% of the maximum data rate, about 2 dB or 37% of power saving can be achieved with the decoupling. Similarly, under the UMa channel environment, about 1.5 dB power saving can be achieved for the same 90% data rate of the

TABLE IV
PERFORMANCE SUMMARY FOR THE SHOWCASES OF THE THREE TYPES OF ANTENNA

	Passive Test						MIMO OTA Performance	
	Isolation		Matching Condition	Total Efficiency		Pattern Change	Power saving in UMi Channel Model	Power saving in UMa Channel Model
	Coupled	Decoupled		Coupled	Decoupled			
IFA	12 dB	29 dB	Improved	68 %	75 %	Small	0.5 dB for 64 QAM	0.3 dB for 16 QAM
Monopole	9 dB	30 dB	Improved	53 %	69 %	Small	2.0 dB for 64 QAM	1.5 dB for 16 QAM
Loop	14 dB	26 dB	Unchanged	50 %	54 %	Small	0.6 dB for 16 QAM	1.2 dB for 16 QAM

*The isolation and total efficiency is compared at 2.14 GHz and the MIMO OTA test is operated in the 10 MHz band (2.135- 2.145 GHz).

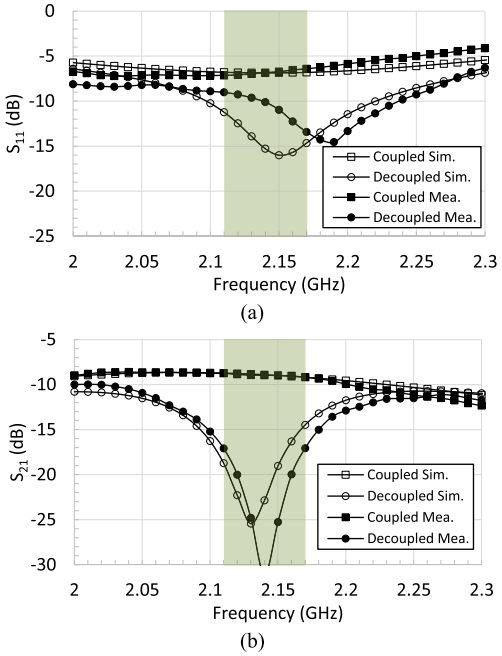

Fig. 12. Simulated and measured S-parameters of the coupled and decoupled monopole antennas. (a) $|S_{11}|$. (b) $|S_{21}|$.

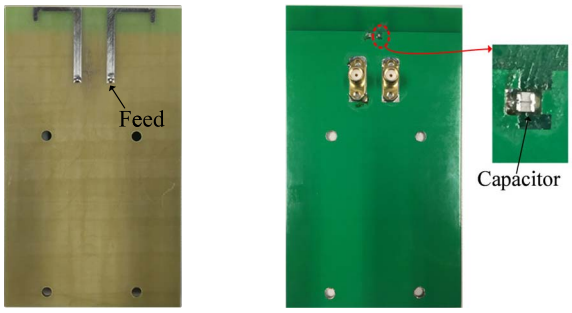

Fig. 13. Prototype of the pair of decoupled monopole antennas. (a) Front view. (b) Back view with the zoomed-in view of one of the soldered capacitors (note that two shunt-connected SMD capacitors are used to realize one capacitor).

maximum value. Similar to the case of IFAs, the radiation patterns do not significantly change after decoupling, but the total efficiency improvement is noticeable.

D. Two Loop Antennas

A loop antenna is another commonly used antenna type in mobile terminals. It is well known that the loop antenna is less vulnerable to the body proximity effect since the current induced on the ground plane is weak. To show the applicability of the proposed decoupling method on loop antennas, as shown in Fig. 14(a), two identical loop antennas that are placed antisymmetrically on the two opposite edges of the PCB board are considered. The dimensions of a loop antenna, as well as a reentrant opening for inlaying a decoupling capacitor, are marked in Fig. 14(b) with the specific values listed in Table II. For the chosen locations for inlaying decoupling capacitors and the dimensions for the short stub, the contour plot of mutual coupling at 2.14 GHz with respect to C_1 and C_2 can be obtained and is shown in Fig. 15. According to the contour plot, two 1.1 pF capacitors are chosen in EM simulation after fine-tuning. The simulated and measured S_{11} and S_{21} of the coupled and the decoupled loop antennas are presented in

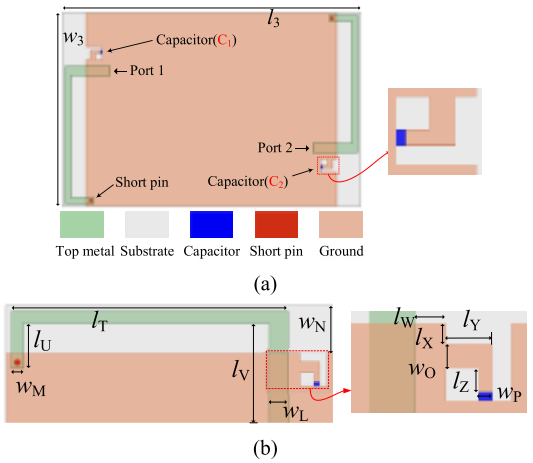

Fig. 14. Configuration of two loop antennas. (a) Top view. (b) Dimensions.

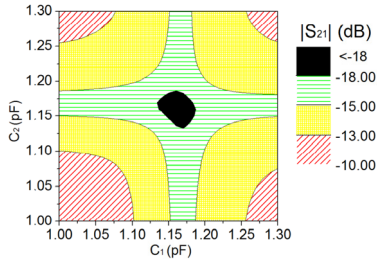

Fig. 15. Contour plot of mutual coupling S_{21} with respect to C_1 and C_2 for the two loop antennas.

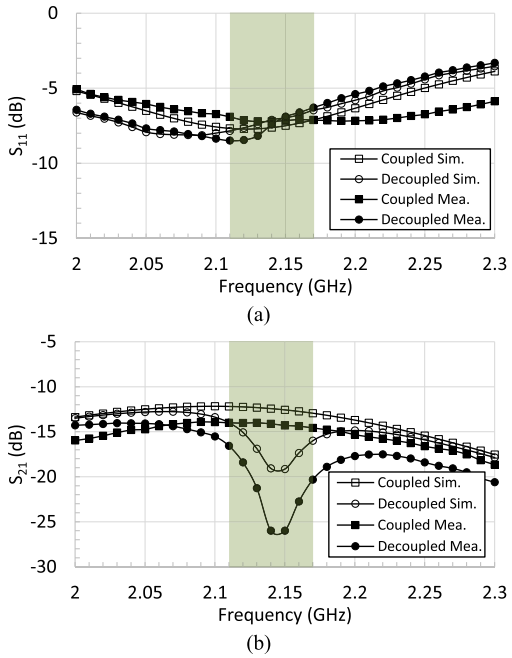

Fig. 16. Simulated and measured S-parameters of the coupled and decoupled loop antennas. (a) $|S_{11}|$. (b) $|S_{21}|$.

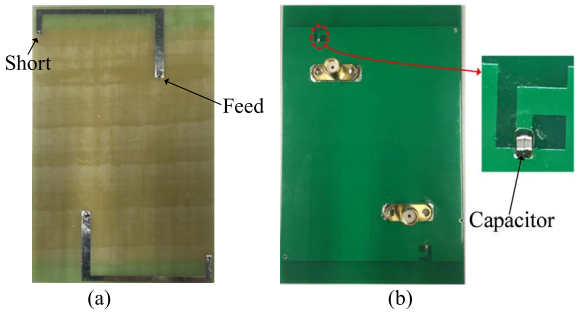

Fig. 17. Prototype of the decoupled loop antennas. (a) Top view. (b) Bottom view.

Fig. 16(a) and (b), respectively. It can be seen that the isolation is improved from about 14 to 26 dB at 2.14 GHz, and the matching condition is almost unchanged. Fig. 17 shows the fabricated prototype of the decoupled loop antennas.

As summarized in Table III, the multiplexing efficiency at 2.14 GHz is improved from 45.6% to 49.1% after decoupling. The average throughputs for the LTE module with the coupled and decoupled loop antennas are measured under the UMi and UMa environments. As shown in Table IV, in the UMi channel environment, for the same 90% data rate of the maximum value of 14.386 Mb/s, about 0.6 dB or 13% of power saving can be achieved after decoupling. Similarly, under the UMa channel environment, about 1.2 dB power saving can be achieved. Again, it is found that the radiation patterns do not significantly change after decoupling.

E. Four MIMO Antennas of Different Types

To demonstrate that the proposed self-curing decoupling method works for the MIMO array antennas with more than

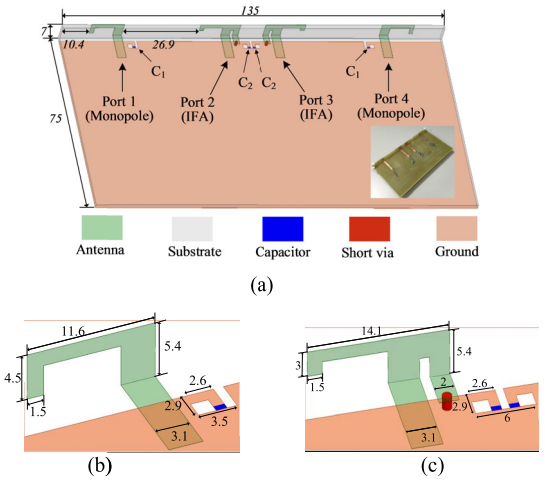

Fig. 18. Configuration of a four-element array (a prototype is inserted). (a) Full view. (b) Monopole antenna element. (c) IFA element. The unit used is millimeters.

two antenna elements, decoupling of four MIMO antennas, as shown in Fig. 18(a), is showcased. The MIMO antenna array contains two IFAs and two monopole antennas, all working at 3.5 GHz frequency band. The dimensions of the IFA and monopole antenna are marked in Fig. 18(b) and (c).

Owing to the symmetry of the array, mutual coupling exhibits certain symmetry, say $S_{21} = S_{43}$ and $S_{31} = S_{42}$. Therefore, only two kinds of capacitors, C_1 and C_2, as shown in Fig. 18(a), need to be determined. By adopting the nonlinear least square scheme discussed in Section II, the cost function can be defined as follows:

$$\min_{\boldsymbol{C}} ||F(\boldsymbol{C})||_2^2 = \min_{\boldsymbol{C}} (|S_{12}(\boldsymbol{C})|^2 + |S_{13}(\boldsymbol{C})|^2 + |S_{14}(\boldsymbol{C})|^2 + |S_{23}(\boldsymbol{C})|^2 + |S_{24}(\boldsymbol{C})|^2 + |S_{34}(\boldsymbol{C})|^2) \tag{4}$$

Using the nonlinear least square optimization method provided in MATLAB, the two capacitors can be found as $C_1 = 0.64$ pF and $C_2 = 0.53$ pF. Then the antenna array is fabricated using FR4 PCB boards, and $C_1 = 0.6$ pF and $C_2 = 0.5$ pF are used in the measurement. As shown in Fig. 19, the six mutual couplings are all reduced by more than 10 dB at 3.5 GHz: S_{21} and S_{43} are reduced from -10 to -20.6 dB; S_{32} from -14 to -30 dB; S_{31} and S_{42} from -17 to -32 dB; and S_{41} from -20 to -37 dB. Additionally, the matching condition at port 1 is significantly improved and that at port 2 does not deteriorate after decoupling. Similar to the cases of two-element arrays, the measured total efficiency of the four-element array is improved from 62.5% to 70% after decoupling.

This example demonstrates that all three different mutual couplings between one element and three others can be simultaneously mitigated using the matrix diagonalization model presented in Section II. The decoupling method shows no discrimination on the antenna type.

The proposed decoupling method is a more general technique than the method proposed in [27], which only works for IFAs, in two aspects: 1) it is applicable not only to IFAs but also to monopole and loop antennas and 2) it works not only

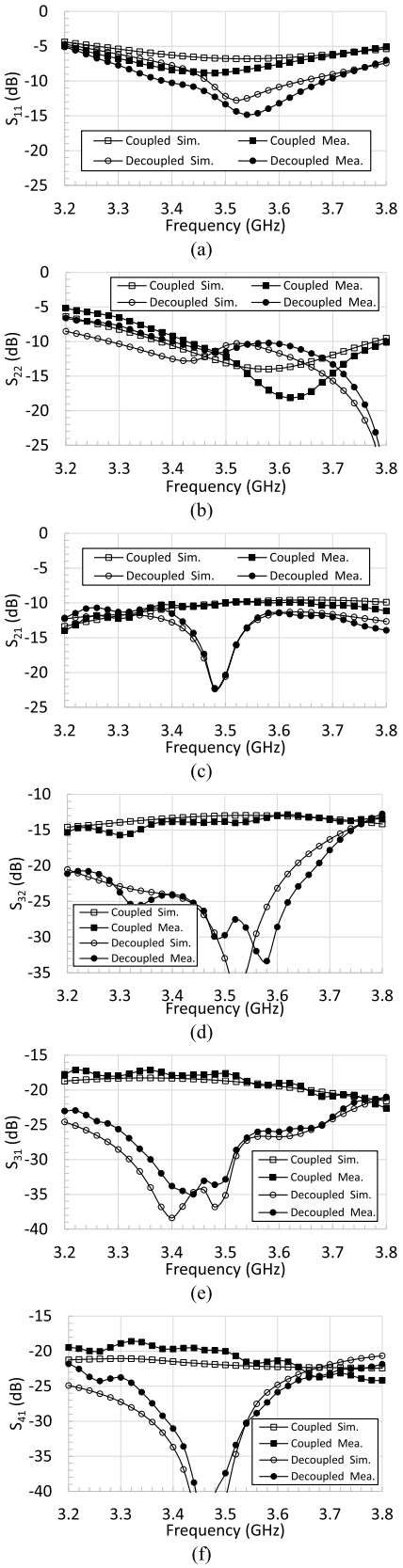

Fig. 19. Simulated and measured S-parameters of the four-element array. (a) S_{11}. (b) S_{22}. (c) S_{21}. (d) S_{32}. (e) S_{31}. (f) S_{41}.

for two-element arrays but also for MIMO arrays with a higher number of elements. Additionally, the matrix diagonalization method proposed in this article is effective to the decoupling

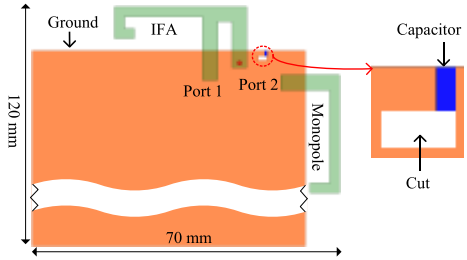

Fig. 20. Configuration of the coupled IFA and monopole antenna example.

problems of a MIMO array that contains a high number of elements using unequal-value capacitors.

IV. Physical Mechanism

Although multiple showcases have demonstrated the effectiveness of the proposed decoupling method, a convincing interpretation that reveals its working mechanism would be more interesting to many researchers. To prove the generality of this decoupling method, an illustrative example of decoupling an IFA and a monopole antenna using a single capacitor, as shown in Fig. 20, is studied using the in-house PEEC simulator. PEEC is a classic EM model that converts an EM problem into a circuit domain representation, which is more rudimentary to engineers.

The dimensional variables in Fig. 3(b) are used for the IFA in the illustrative example and those in Fig. 10(b) are used for the monopole antenna and the reentrant opening on the ground. In this example, dimensional variables l_{A}, l_{D}, l_{G}, l_{M}, l_{P}, l_{Q}, l_{S}, w_{I}, and w_{K} are assigned to 27, 5, 17, 24, 81, 2.3, 2, 7, and 1.8, all in millimeters, respectively. For the sake of clarity, only one decoupling capacitor is used. The EM simulated and measured results for the coupled and decoupled cases as shown in Fig. 21 justify that by positioning an "acupoint" near the shorting arm of the IFA and inlaying a capacitor of 2.6 pF on the ground plane can improve the isolation of the two antennas from 9 to 21 dB at 2.14 GHz while maintaining matching conditions of the two antennas for better than 10 dB.

Since the reentrant opening cut is electrically small, it can be easily verified by EM simulation that the opening cut does not change the antenna characteristics. Therefore, in the following discussion, the coupled antennas with the opening cut on the ground are used to represent the original coupled antennas for easy explanation.

A convincing interpretation of the working mechanism can be given using the changes in current distributions in the four scenarios presented in Fig. 22. In Fig. 22(a), port 1 is excited by an ideal current source I_1 and port 2 is terminated with a 50 Ω load. In this case, a current at port 2 due to mutual coupling is induced and is denoted as I_2. Fig. 22(b) shows the decoupled case with the decoupling capacitor C_1 inlaid, in which port 1 is also excited by the current source I_1, and the induced current at port 2 is denoted as I_2', whose value is next to zero. In the PEEC model, the current flowing through capacitor C_1 can be measured and is denoted as I_{C1}.

Assume the current distributions over the antennas and the ground plane for the coupled and decoupled cases, shown in Fig. 22(a) and (b), respectively, are $\boldsymbol{J}_c$ and $\boldsymbol{J}_d$, respectively.

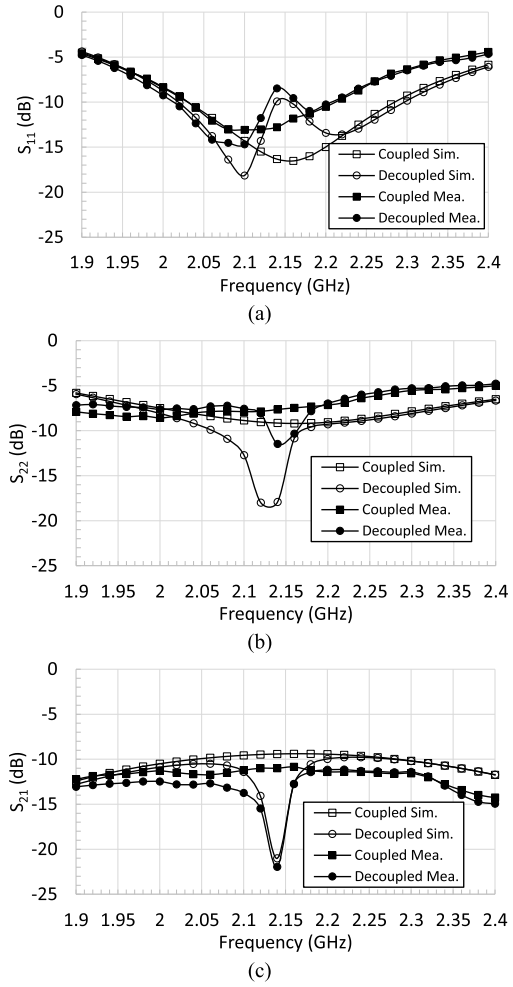

Fig. 21. Simulated and measured S-parameters of the coupled and decoupled IFA and monopole antenna. (a) $|S_{11}|$. (b) $|S_{22}|$. (c) $|S_{21}|$.

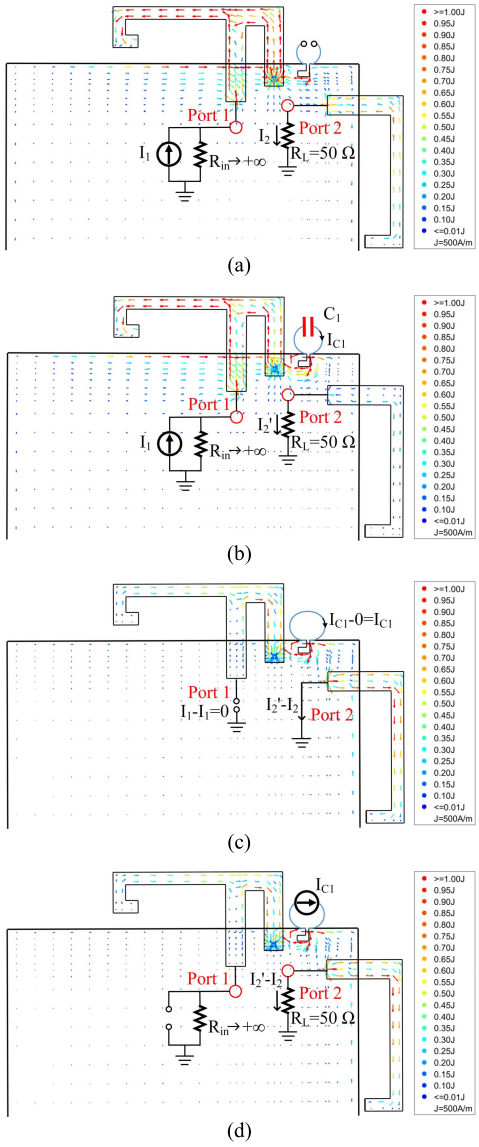

Fig. 22. Simulated current density distribution. (a) Coupled antennas. (b) Decoupled antennas. (c) Difference current. (d) Excited by I_{C1} at acupoint with port 1 open and port 2 terminated with a 50 Ω load.

It would be interesting to investigate the incremental current $\delta \boldsymbol{J} = \boldsymbol{J}_d - \boldsymbol{J}_c$, as shown in Fig. 22(c), which states that if only the incremental current exists over the coupled antenna system, the current through the reentrant opening would be I_{C1}, the current entering port 1 would be zero (open circuit), and the current at port 2 would be $I_2' - I_2$, which approximately equals to $-I_2$. In other words, placing an appropriate coherent current source at the reentrant opening can generate an interference signal that is opposite to the coupled signal at the coupled port so that the coupled signal is canceled.

To verify the aforementioned observation, capacitor C_1 is replaced with an ideal current source whose value is I_{C1} in the PEEC model. With port 2 terminated by a 50 Ω load and port 1 set to open circuit, it is found that the current at port 2 numerically equals to $I_2' - I_2 \approx -I_2$. Fig. 22(d) shows the PEEC simulation setup and the current distribution of this scenario. It can be seen that the current distributions in Fig. 22(c) and (d) are identical. This numerical experiment verifies that the inlaid capacitor on the ground plane naturally creates a coherent current source at the "acupoint" that generates a signal at the victim port with the same magnitude but opposite phase as that of the coupled signal, resulting in mutual coupling cancelation.

V. Conclusion

This article presents a self-curing decoupling technique for mitigating mutual coupling among MIMO antennas of commonly-used types for mobile terminals. Compared with the method in [27] that is only applicable to IFAs, the uniqueness of this new self-curing decoupling method is fourfold: 1) it not only works for IFA but also works well for monopole and loop antennas, and any combination of them; 2) it tends to improve the matching conditions of the decoupled antennas with a wider working bandwidth without any extra impedance matching circuit; 3) it is highly flexible in implementation in terms of the number and the position of the decoupling capacitors; and importantly 4) the method works well for MIMO antenna arrays with more than two antenna elements.

In this article, the generality of the proposed decoupling technique has been demonstrated through three types of commonly used antennas of two elements for mobile terminals, namely IFA, monopole, and loop antennas. One decoupling example with four antenna elements of different types is also given to demonstrate its applicability to an array with a high number of elements. The design procedure is illustrated by two approaches: 1) a graphical solution with a user-defined specification, which is highly effective for an array with two elements and 2) a matrix diagonalization method, which is very useful for an array with more than two antenna elements. The physical mechanism of the decoupling method is revealed by PEEC modeling. Practically, the impact of the decoupling method to MIMO wireless terminals has been demonstrated through extensive MIMO OTA tests in a controllable multipath channel environment. A significant improvement in the measured data throughput justifies the usefulness of the new self-curing decoupling technique.

REFERENCES

[1] Z. Ying, "Antennas in cellular phones for mobile communications," *Proc. IEEE*, vol. 100, no. 7, pp. 2286–2296, Jul. 2012.

[2] X. Mei and K.-L. Wu, "How low does mutual coupling need to be for MIMO antennas," in *Proc. IEEE Int. Symp. Antennas Propag. USNC/URSI Nat. Radio Sci. Meeting*, Boston, MA, USA, Jul. 2018, pp. 1579–1580.

[3] M. A. Jensen and J. W. Wallace, "A review of antennas and propagation for MIMO wireless communications," *IEEE Trans. Antennas Propag.*, vol. 52, no. 11, pp. 2810–2824, Nov. 2004.

[4] F. M. Barradas, P. M. Tomé, J. M. Gomes, T. R. Cunha, P. M. Cabral, and J. C. Pedro, "Power, linearity, and efficiency prediction for MIMO arrays with antenna coupling," *IEEE Trans. Microw. Theory Techn.*, vol. 65, no. 12, pp. 5284–5297, Dec. 2017.

[5] M. Pelosi, M. B. Knudsen, and G. F. Pedersen, "Multiple antenna systems with inherently decoupled radiators," *IEEE Trans. Antennas Propag.*, vol. 60, no. 2, pp. 503–515, Feb. 2012.

[6] M.-Y. Li *et al.*, "Eight-port orthogonally dual-polarized antenna array for 5G smartphone applications," *IEEE Trans. Antennas Propag.*, vol. 64, no. 9, pp. 3820–3830, Sep. 2016.

[7] A. Diallo, C. Luxey, P. Le Thuc, R. Staraj, and G. Kossiavas, "Study and reduction of the mutual coupling between two mobile phone PIFAs operating in the DCS1800 and UMTS bands," *IEEE Trans. Antennas Propag.*, vol. 54, no. 11, pp. 3063–3073, Nov. 2006.

[8] S.-W. Su, C.-T. Lee, and F.-S. Chang, "Printed MIMO-antenna system using neutralization-line technique for wireless USB-dongle applications," *IEEE Trans. Antennas Propag.*, vol. 60, no. 2, pp. 456–463, Feb. 2012.

[9] A. C. K. Mak, C. R. Rowell, and R. D. Murch, "Isolation enhancement between two closely packed antennas," *IEEE Trans. Antennas Propag.*, vol. 56, no. 11, pp. 3411–3419, Nov. 2008.

[10] B. K. Lau and J. B. Andersen, "Simple and efficient decoupling of compact arrays with parasitic scatterers," *IEEE Trans. Antennas Propag.*, vol. 60, no. 2, pp. 464–472, Feb. 2012.

[11] L. Zhao and K.-L. Wu, "A decoupling technique for four-element symmetric arrays with reactively loaded dummy elements," *IEEE Trans. Antennas Propag.*, vol. 62, no. 8, pp. 4416–4421, Aug. 2014.

[12] H. Xu, H. Zhou, S. Gao, H. Y. Wang, and Y. J. Cheng, "Multimode decoupling technique with independent tuning characteristic for mobile terminals," *IEEE Trans. Antennas Propag.*, vol. 65, no. 12, pp. 6739–6751, Dec. 2017.

[13] C.-Y. Chiu, C.-H. Cheng, R. D. Murch, and C. R. Rowell, "Reduction of mutual coupling between closely-packed antenna element," *IEEE Trans. Antennas Propag.*, vol. 55, no. 6, pp. 1732–1738, Jun. 2007.

[14] S. Zhang, B. K. Lau, Y. Tan, Z. Ying, and S. He, "Mutual coupling reduction of two PIFAs with a T-shape slot impedance transformer for MIMO mobile terminal," *IEEE Trans. Antennas Propag.*, vol. 60, no. 3, pp. 1521–1531, Mar. 2012.

[15] F. Yang and Y. Rahmat-Samii, "Microstrip antennas integrated with electromagnetic band-gap (EBG) structures: A low mutual coupling design for array applications," *IEEE Trans. Antennas Propag.*, vol. 51, no. 10, pp. 2936–2946, Oct. 2003.

[16] L. Yang, M. Fan, F. Chen, J. She, and Z. Feng, "A novel compact electromagnetic-bandgap (EBG) structure and its applications for microwave circuits," *IEEE Trans. Microw. Theory Techn.*, vol. 53, no. 1, pp. 183–190, Jan. 2005.

[17] J. Andersen and H. Rasmussen, "Decoupling and descattering networks for antennas," *IEEE Trans. Antennas Propag.*, vol. AP-24, no. 6, pp. 841–846, Nov. 1976.

[18] J. Sui and K.-L. Wu, "A general T-stub circuit for decoupling of two dual-band antennas," *IEEE Trans. Microw. Theory Techn.*, vol. 65, no. 6, pp. 2111–2121, Jun. 2017.

[19] S. C. Chen, Y. S. Wang, and S. J. Chung, "A decoupling technique for increasing the port isolation between two strongly coupled antennas," *IEEE Trans. Antennas Propag.*, vol. 56, no. 12, pp. 3650–3658, Dec. 2008.

[20] H. Meng and K.-L. Wu, "An LC decoupling network for two antennas working at low frequencies," *IEEE Trans. Microw. Theory Techn.*, vol. 65, no. 7, pp. 2321–2329, Jul. 2017.

[21] C. Volmer, J. Weber, R. Stephan, K. Blau, and M. A. Hein, "An eigenanalysis of compact antenna arrays and its application to port decoupling," *IEEE Trans. Antennas Propag.*, vol. 56, no. 2, pp. 360–370, Feb. 2008.

[22] J. C. Coetzee and Y. Yu, "Port decoupling for small arrays by means of an eigenmode feed network," *IEEE Trans. Antennas Propag.*, vol. 56, no. 6, pp. 1587–1593, Jun. 2008.

[23] L. K. Yeung and Y. E. Wang, "Mode-based beamforming arrays for miniaturized platforms," *IEEE Trans. Microw. Theory Techn.*, vol. 57, no. 1, pp. 45–52, Jan. 2009.

[24] L. Zhao, L. K. Yeung, and K.-L. Wu, "A coupled resonator decoupling network for two-element compact antenna arrays in mobile terminals," *IEEE Trans. Antennas Propag.*, vol. 62, no. 5, pp. 2767–2776, May 2014.

[25] L. Zhao, K.-W. Qian, and K.-L. Wu, "A cascaded coupled resonator decoupling network for mitigating interference between two radios in adjacent frequency bands," *IEEE Trans. Microw. Theory Techn.*, vol. 62, no. 11, pp. 2680–2688, Nov. 2014.

[26] K. Qian, L. Zhao, and K.-L. Wu, "An LTCC coupled resonator decoupling network for two antennas," *IEEE Trans. Microw. Theory Techn.*, vol. 63, no. 10, pp. 3199–3207, Oct. 2015.

[27] J. Sui and K.-L. Wu, "Self-curing decoupling technique for two inverted-F antennas with capacitive loads," *IEEE Trans. Antennas Propag.*, vol. 66, no. 3, pp. 1093–1101, Mar. 2018.

[28] M. V. Group and P. France. *StarMIMO*. Accessed: Sep. 29, 2019. [Online]. Available: http://www.mvg-world.com/en/products/field_product_family/antenna-measurement-2/starmimo

[29] CTIA. *Test Plan for 2×2 Downlink MIMO and Transmit Diversity Over-the-Air Performance*. Accessed: Sep. 29, 2019. [Online]. Available: https://api.ctia.org/wp-content/uploads/2018/05/ctia_mimo_ota_tp_v1_2.pdf

[30] C. A. Balanis, *Antenna Theory: Analysis and Design*. Hoboken, NJ, USA: Wiley, 2012, pp. 64–65.

[31] S. Zhang, S. Khan, and S. He, "Reducing mutual coupling for an extremely closely-packed tunable dual-element PIFA array through a resonant slot antenna formed in-between," *IEEE Trans. Antennas Propag.*, vol. 58, no. 8, pp. 2771–2776, Aug. 2010.

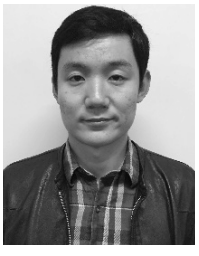

Jiangwei Sui received the B.S. degree from the University of Science and Technology of China (USTC), Hefei, China, in 2014 and the Ph.D. degree from The Chinese University of Hong Kong, Hong Kong, in 2019.

He is currently with Vivo Communication Technology Co., Ltd., as an Antenna Engineer. His current research interests include microwave theory, antenna theory, antenna design, and antenna array decoupling technique for mobile communication systems.

Yuhang Dou (S'13) received the B.S. degree in electronic engineering from the Nanjing University of Science and Technology, Nanjing, China, in 2012 and the Ph.D. degree from The Chinese University of Hong Kong, Hong Kong, in 2019.

Her current research interests include physics-based circuit-domain modeling methods for radiation problems and signal integrity (SI) analysis of high-speed large-scale interconnection and packaging problems.

Dr. Dou was a recipient of the Fist Runner Up Awards in both 2015 and 2018 IEEE Hong Kong AP/MTT Postgraduate Conferences.

Xide Mei received the B.S. degree in electronic engineering from the University of Electronic Science and Technology of China, Chengdu, China, in 2015. He is currently pursuing the Ph.D. degree with The Chinese University of Hong Kong, Hong Kong.

His current research interests include antenna design, wireless channel modeling, and the design of multiple-input multiple-output antenna array by incorporating wireless channel models.

Ke-Li Wu (M'90–SM'96–F'11) received the B.S. and M.Eng. degrees from the Nanjing University of Science and Technology, Nanjing, China, in 1982 and 1985, respectively, and the Ph.D. degree from Laval University, Quebec, QC, Canada, in 1989.

From 1989 to 1993, he was a Research Engineer with McMaster University, Hamilton, ON, Canada. He joined the Corporate Research and Development Division, COM DEV (currently Honeywell Aerospace), Cambridge, ON, Canada, in 1993, where he was a Technical Staff Principal Member. Since 1999, he has been with The Chinese University of Hong Kong, Hong Kong, where he is currently a Professor and the Director of the Radiofrequency Radiation Research Laboratory. His current research interests include EM-based circuit domain modeling of high-speed interconnections, robot automatic tuning of microwave filters, decoupling techniques of MIMO antennas, and the Internet of Things technologies.

Dr. Wu is a member of the IEEE MTT-8 Subcommittee. He serves as a TPC member for many prestigious international conferences. He was a recipient of the 1998 COM DEV Achievement Award and the Asia–Pacific Microwave Conference Prize twice in 2008 and 2012, respectively. He was an Associate Editor of the IEEE TRANSACTIONS ON MICROWAVE THEORY AND TECHNIQUES (MTT) from 2006 to 2009.